

# ***a* and *b* waves detection in acceleration photoplethysmogram**

**Mohamed Elgendi**

Department of Computing Science, University of Alberta, Canada

E-mail: [moe.elgendi@gmail.com](mailto:moe.elgendi@gmail.com)

## **Abstract**

An efficient and robust method based on two moving average filters followed by a dynamic event duration threshold has been developed to detect *a* and *b* waves in the acceleration photoplethysmogram signals. The detection of *a* and *b* waves is affected by the quality of the photoplethysmogram recordings, especially for the heat stressed collection. The developed a method detects *a* and *b* waves in Arrhythmia APG Signals that suffer from: 1) non-stationary effects, 2) low signal-to-noise ratio, The performance of the proposed method was tested on 27 records collected in normal and heat-stressed conditions resulting in 99.68 percent sensitivity and 99.57 percent positive predictivity.

Keywords: acceleration photoplethysmogram, *a* wave detection, *b* wave detection, heat stress signal analysis

## **1. Introduction**

It has been shown that atherosclerosis, the underlying cause of coronary heart disease, can occur even in children and adolescents. (Kimm et al.[1]; Strong et al. [2].; Leeson et al [3].). This fact leads to the belief that the primary prevention of atherosclerosis should commence in childhood. Monitoring arterial vascular walls as well as risk factors such as hypertension, hypercholesterolemia and other blood biochemical profiles can potentially help to identify individuals having an increased risk of developing atherosclerosis in adulthood.

Pulse-wave analysis has been shown to provide valuable information on aortic stiffness and elasticity (Chrife et al.[4]; Kelly et al.[5], O'Rourke et al.[6]), and it has been widely used to evaluate the vascular effects of aging, hypertension and atherosclerosis (Darne et al.[7]; Kelly et al.[8], Takazawa et al. [9]; Bortolotto et al.[10]).

Photoelectric plethysmography, also known as photoplethysmography and its acronym in some literature, is (PPG/PPG) and when it is called digital volume pulse, the acronym is (DVP). In this paper, the abbreviation PPG is going to be used according to Elgendi's recommendation [11].

Fingertip photoplethysmography mainly reflects the pulsatile volume changes in the finger arterioles, has been recognized as a noninvasive method of measuring arterial pulse waves in relation to changes in wave amplitude (Fichett [12]). However, the wave contour itself has not been analysed because of the difficulty in detecting minute changes in the phase of the inflections. Previous attempts at PPG analysis showed that such delicate changes in the waves were emphasized and easily quantified by quadratically differentiating the original PPG signal

with respect to time (Seki [13]; Ozawa [14]). Accordingly, the second derivative of the PPG (APG) was developed as a method allowing more accurate recognition of the inflection points and easier interpretation of the original plethysmogram wave. In this paper, the abbreviation APG for the second derivative photoplethysmogram will be used based on Elgendi's recommendation [11].

As shown in Fig.1, The waveform of the APG consists of four systolic waves (*a*, *b*, *c* and *d* waves) and one diastolic wave (*e* wave) Takazawa et al.[15]. The height of each wave was measured from the baseline, with the values above the baseline being positive and those under it negative.

This convenient and objective technique for analyzing the PPG wave has recently been performed more frequently than the conventional recordings. Several epidemiological studies have demonstrated that the information extracted from the APG waveform is associated closely with age and other risk factors for atherosclerotic vascular disease (Takada et al. [16]; Imanaga et al. [17]; Takazawa et al. [9]).

Although the clinical significance of APG measurement has been thoroughly discussed, there is still a lack of studies focusing on the automatic detection of *a*, *b* waves in APG signals.

Therefore this investigation, the first of its kind, aimed to develop a fast and robust algorithm to detect *a*, *b* waves in APG signals.

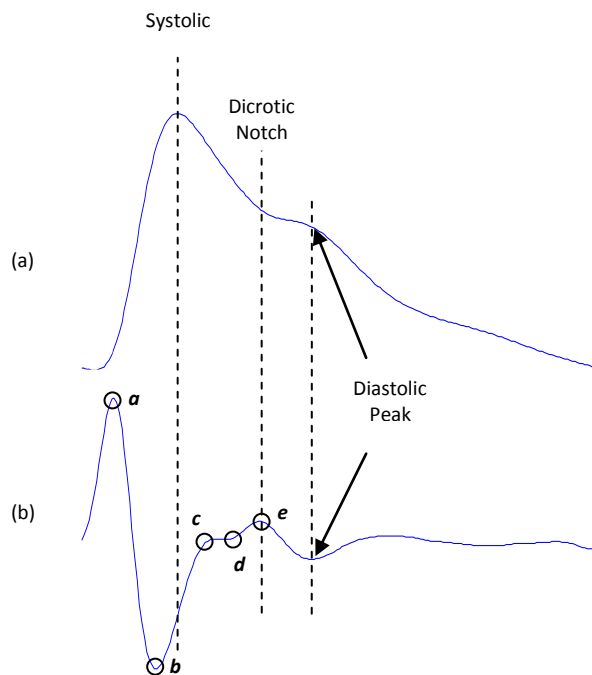


**Figure 1 Signal Measurements [18]** (a) fingertip photoplethysmogram (b) second derivative wave of photoplethysmogram. The photoplethysmogram waveform consists of one systolic wave and one diastolic wave while the second derivative photoplethysmogram waveform consists of four systolic waves (*a*, *b*, *c*, and *d* waves) and one diastolic wave (*e* wave).

The APG waveform was measured in a population-based sample of healthy males. Heat stress exercise changes the APG waveform pattern and as consequence will affect the detection of *a* and *b* waves. Because of the low amplitude of *a* or *b* waves, distinguishing the morphology of *a* or *b* waves in noisy APG signals is considered challenging. However, there was an a serious attempt in 2009 by Matsuyama [19] to detect *a* waves in APG signals using nine QRS algorithms of Friesen's ECG algorithms [20] after modifying the sampling rates and threshold values. The detection rate was below 63 per cent for all nine algorithms when tested on the PPG–Army Heat Stress Dataset. Matsuyama [19] observed that ‘a new algorithm should be more robust against noise and should be applicable to both APG and ECG signals’. Therefore, this investigation aims to develop a numerically efficient and robust algorithm to detect *a* and *b* waves in APG signals.

## 2. Data

There are currently no standard PPG databases available to evaluate the developed algorithms. However, Charles Darwin University has a PPG dataset measured at rest and after exercise, as shown in Figure 2. Two independent annotators annotated *a* and *b* waves in APG signal.

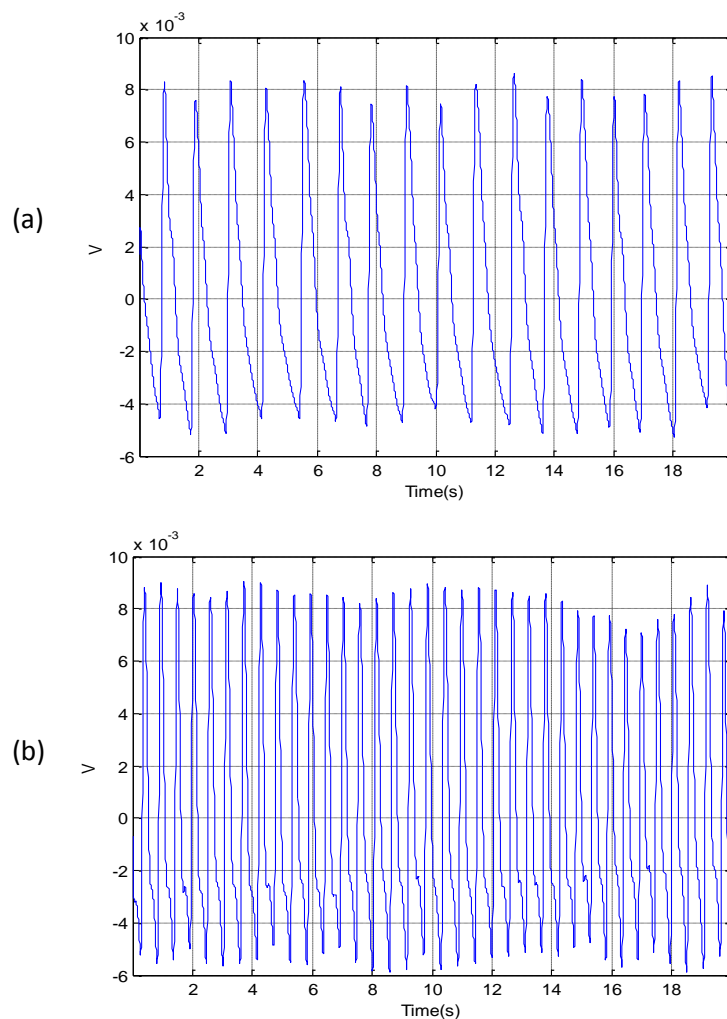


**Figure 2 PPG signals: 20-seconds recording for the same volunteer, measured (a) at rest and (b) after exercise.** It is clear that the heart rate after exercise is higher than at rest. This issue makes it challenging to detect heartbeats from APG signals.

The PPG data were collected as a minor part of a joint project between Charles Darwin University, the Defence Science and Technology Organisation (DSTO) and the Department of Defence. The background of the entire project can be found in [19].

PPGs of 27 healthy volunteers (males) with a mean $\pm$ SD age of 27 $\pm$ 6.9 were measured using a photoplethysmography device (Salus PPG), with the sensor located at the cuticle of the second digit of the left hand. Measurements were taken while the subject was at rest on a chair. PPG data were collected at a sampling rate of 200Hz. The duration of each data segment is 20 seconds.

Annotations is a difficult task due to inter-annotator discrepancy, as the two annotators will never agree completely on what and how to annotate the  $a$  wave. Despite the annotation process being significantly time-consuming, discrepancies can be found in many records. Three cases will be discussed below to show how the discrepancies were adjudicated:

❖ Case 1:

Annotator 1 agrees with Annotator 2 on all of the  $a$  wave positions within an APG record. When both annotators have no discrepancies, it is an optimal situation.

❖ Case 2:

Both annotators agree on most of the  $a$  wave positions except the first  $a$  wave at far left and the last  $a$  wave at the far right.

❖ Case 3:

Annotator 2 considered these two waves  $a$  waves while Annotator 1 did not.

One annotation file has been saved to present the two annotated  $a$  waves by considering the  $a$  waves that have been missed by one of the annotators, or perhaps isolating  $a$  wave that is not consistent with the beat rhythm within the APG recording. The same process applied to  $b$  wave.

### 3. Methodology

The proposed  $a$  and  $b$  waves detection algorithm consists of three main stages: pre-processing (bandpass filtering, second derivative and squaring), feature extraction (generating potential blocks using two moving averages) and classification (thresholding). The structure of the algorithm is shown in Figure 3.

#### *Bandpass Filter*

To design an efficient bandpass filter, two types of challenging noise are addressed:

- i) **High-frequency noise:** this noise is could be due to the instrumentation amplifiers, the recording system pickup of ambient electromagnetic signals or other noises exist above 7 Hz, as shown in Figure 4 (a). High-frequency noise is usually caused by interference from mains power sources being induced onto the recording leads of the PPG. This phenomenon introduces a sinusoidal component into the recording. In Australia, this component is at a frequency of 50 Hz.
- ii) **Low-frequency noise:** this noise is created by poor contact to the fingertip photo sensor. In addition, variations in temperature and bias in the instrumentation amplifiers can cause baseline drift. Regarding the PPG database used in this paper, the body movement was limited due short measurement time (20 seconds) and the fixed position of the arm during the PPG signal collection.

The low-frequency noise can be removed using a high-pass filter. As shown in Figure 4 (b), the low frequencies that cause baseline wandering exist up to 0.5 Hz.

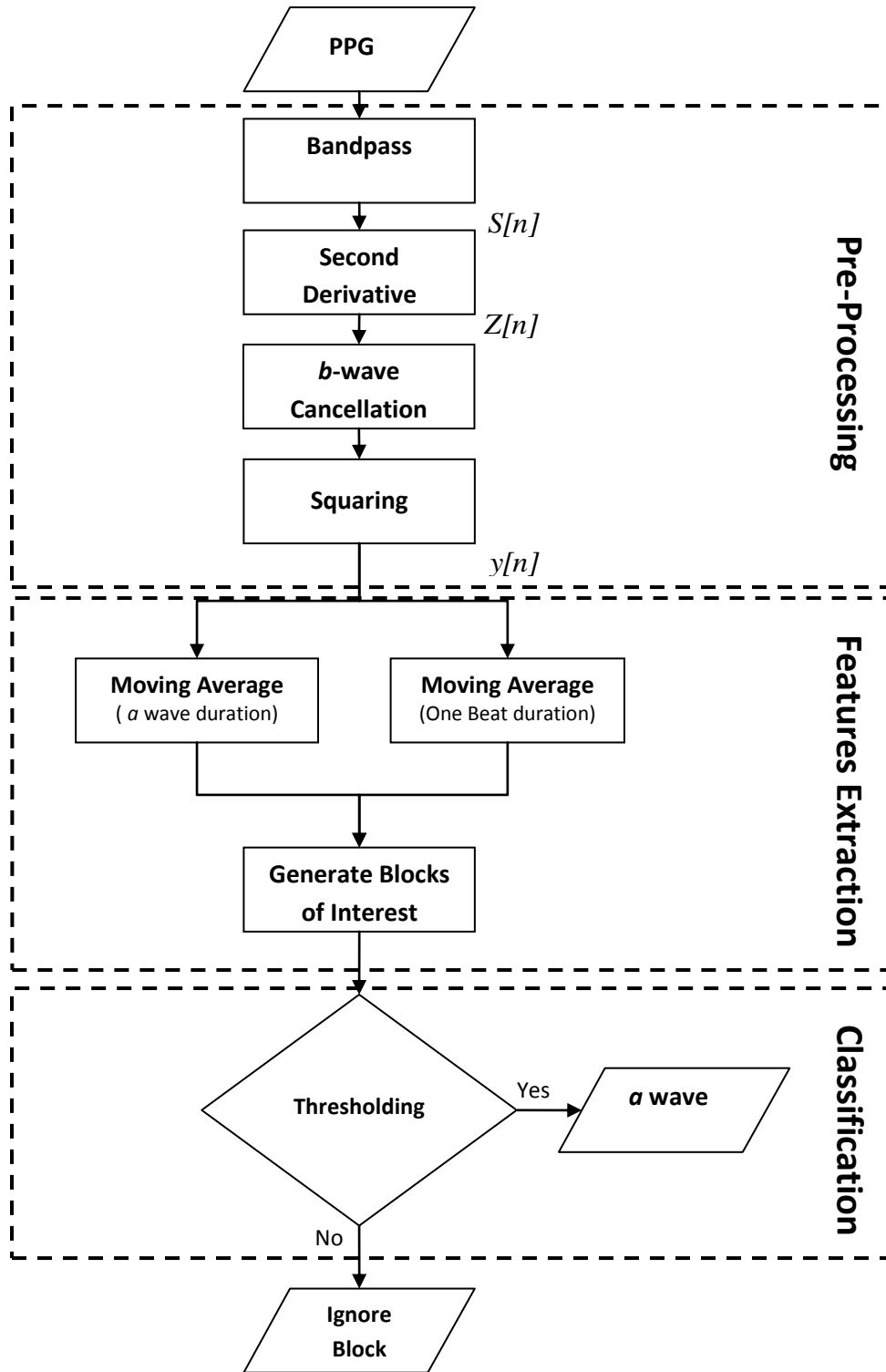


**Figure 3 Flowchart for a new *a* wave detection algorithm.** This *a* wave time-domain detection algorithm consists of three main stages: pre-processing, feature extraction and classification.

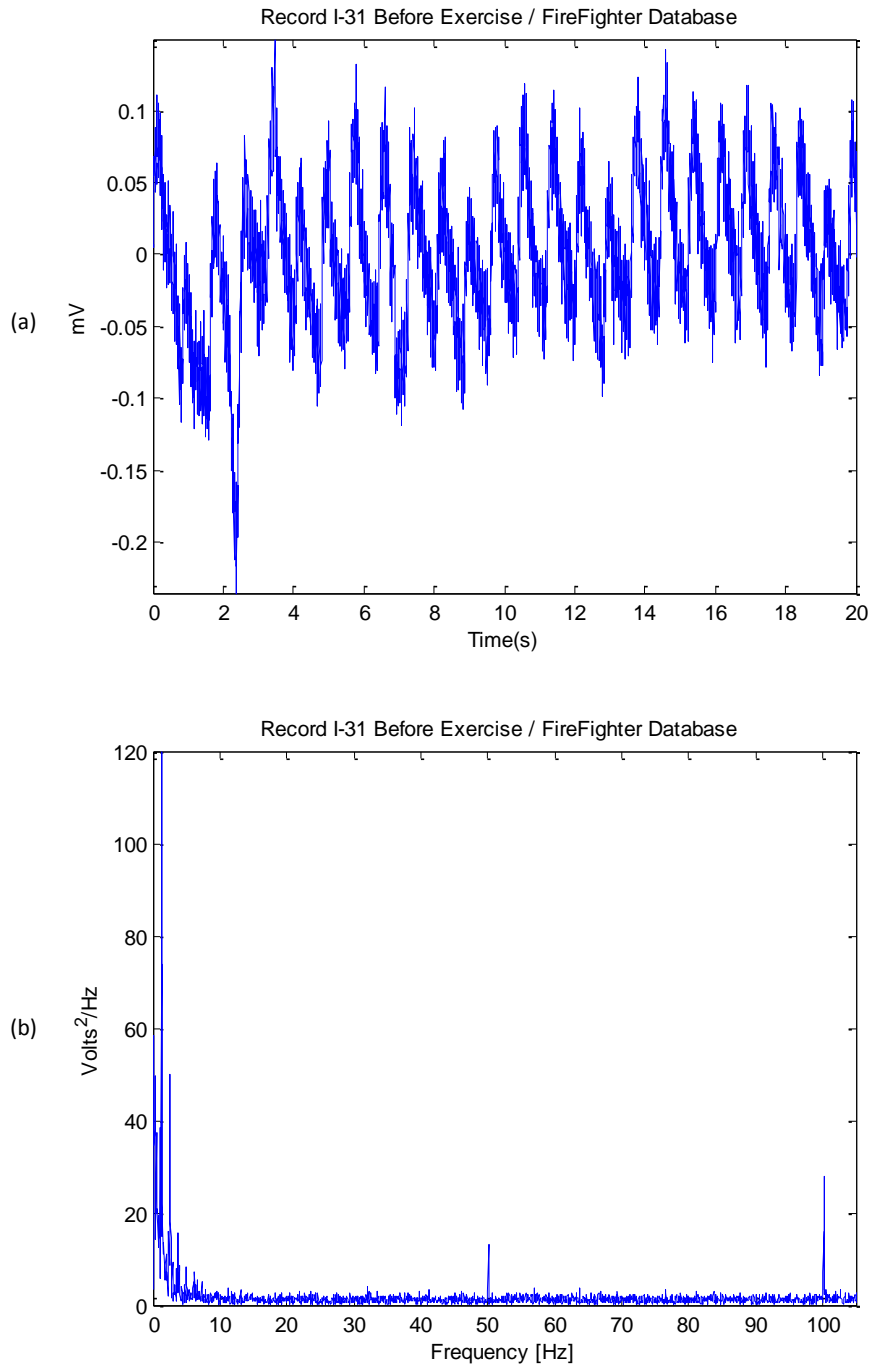


**Figure 4 Demonstrating the PPG signals frequency bands (a) PPG signal, (b) Fourier transform (spectrum) of the PPG signal.** The spectrum illustrates peaks at the fundamental frequency of 50 Hz, as well as the second and third harmonics at 100 Hz respectively. The spectrum shows that the main energy of the PPG signal lies up to 7 HZ.

The periodic interference is clearly displayed as a spike in Figure 4 (b) not only at its fundamental frequency of 50 Hz, but also as spikes at 100 Hz and the higher harmonics.

Extracting the main energy of a and b waves can be done using a bandpass filter which is typically a bidirectional Butterworth implementation [21], as it offers good transition-band characteristics at low coefficient orders making it efficient to implement [21].

A second-order Butterworth filter with bandpass 0.5–7 Hz has implemented by cascading a high- and low-pass filters to remove the baseline wander and high frequencies that do not contribute to the *a* and *b* waves. Since one complete heart cycle takes approximately one second, the frequencies below 0.5 Hz can be considered noise (baseline wander). The 7 Hz is chosen because most of the energy of the PPG signal is below 7 Hz, as shown in Figure 4 (b).

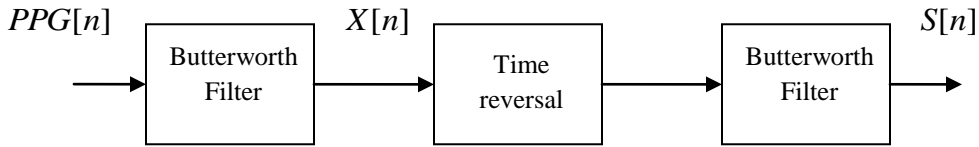


**Figure 5 Demonstrating the zero-phase filtering in PPG signals**

The bidirectional Butterworth filter is implemented as shown in Figure 5. The  $S[n]$  output will be a filtered version of  $PPG[n]$  with no phase distortion. The same Butterworth filter is used twice in this scheme: the time reversal step is a straight left–right flipping of the time-domain sequence, to produce zero-phase filtering, as follows:

$$X[n] = \sum_{k=0}^N b_k PPG[n-k] - \sum_{k=1}^N a_k X[n-k] \quad \text{Eq. 1}$$

$$S[n] = \sum_{k=0}^N b_k X[n-k] - \sum_{k=1}^N a_k S[n-k] \quad \text{Eq. 2}$$

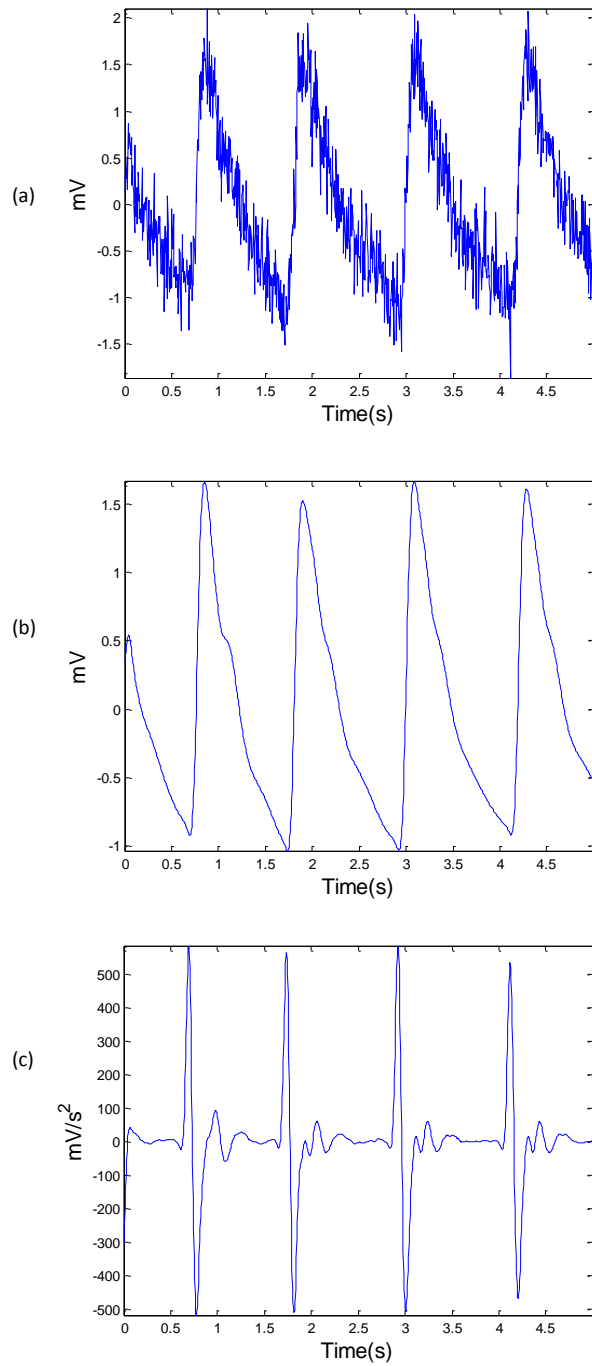


**Figure 6 Algorithm structure for PPG data measured from 'at rest' (Part 1)** (a) Original PPG signal, (b) filtered PPG signal with Butterworth bandpass filter which is  $S[n]$ , (c) second derivative of PPG (APG) which is  $Z[n]$ . (Record B1-Before Exercise / Army database).

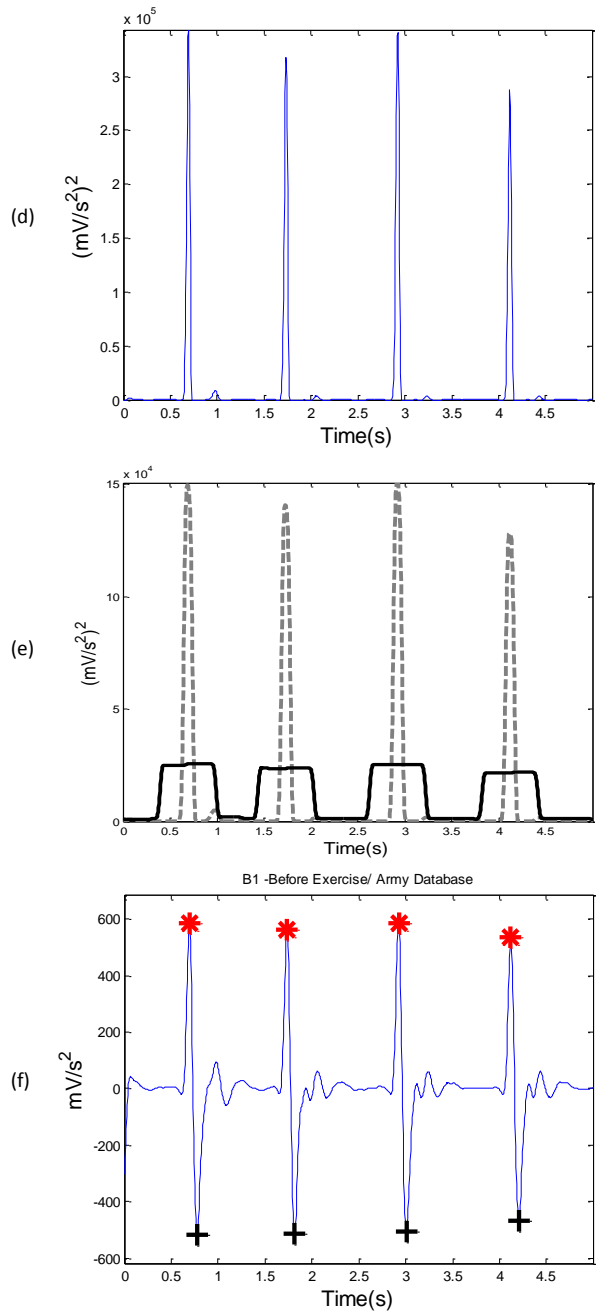


**Figure 7** Algorithm structure for PPG data measured 'at rest' (Part 2) (d) Squaring, (e) generating blocks of interest using two moving averages  $MA_{Peak}$  and  $MA_{OneBeat}$ , (f) the final result of the proposed algorithm to detect  $a$  and  $b$  waves. (record B1: before exercise / army database)

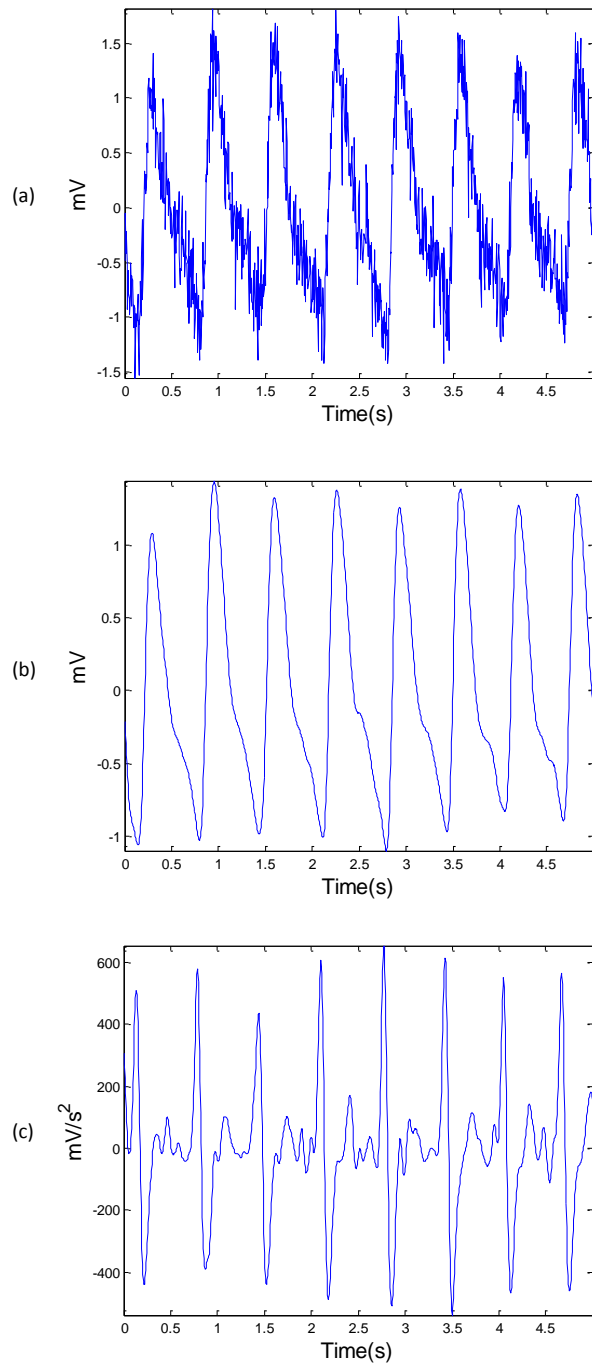


**Figure 8 Algorithm structure for PPG data measured ‘after exercise’ (Part 1)** (a) Original APG signal, (b) filtered PPG signal with Butterworth bandpass filter, which is  $S[n]$  (c) second derivative of PPG (APG), which is  $Z[n]$ . (record C3:after exercise / army database).

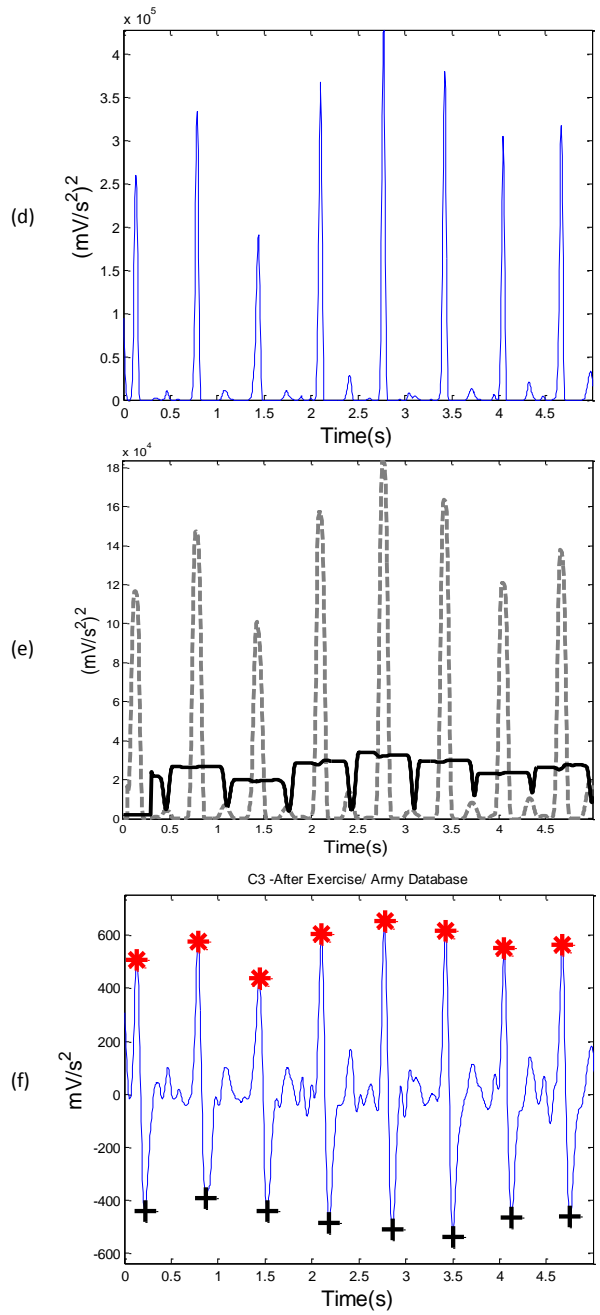


**Figure 9 Algorithm structure for PPG data measured 'after exercise' (Part 2)** (d) Squaring, (e) generating blocks of interest using two moving averages  $MA_{Peak}$  and  $MA_{OneBeat}$ , (f) the final result of the proposed algorithm to detect  $a$  and  $b$  waves. (Record C3: after exercise / army database).

### Second Derivative

To obtain the APG signals  $Z[n]$ , the second derivative will be applied to the filtered PPG  $S[n]$  in order to analyse the APG signals. Equations 3 and 4 represent a non-causal filter; the three-point centre derivative creates with a delay of only two samples.

$$S'[n] = \left. \frac{dS}{dt} \right|_{t=nT} = \frac{1}{2T} (S[n+1] - S[n-1]) \quad \text{Eq. 3}$$

$$Z[n] = \left. \frac{dS'}{dt} \right|_{t=nT} = \frac{1}{2T} (S'[n+1] - S'[n-1]) \quad \text{Eq. 4}$$

where  $T$  is the sampling interval and equals the reciprocal of the sampling frequency, and  $n$  is the number of data points. Figures 6 (c) and 8 (c) show the second derivative of the filtered PPG signal (APG signal) measured at rest and after exercise respectively.

### *b* wave Cancellation

At this stage the *a* wave of the APG needs to be emphasised to distinguish it clearly for detection. This can be done by setting the negative parts of the signal equal to zero

**IF**  $Z[n] < 0$  **THEN**

$$Z[n] = 0$$

**END**

### Squaring

Squaring emphasises large differences resulting from the *a*-wave segment; the small differences arising from *c*, *e* and *d* waves are suppressed:

$$y[n] = (Z[n])^2 \quad \text{Eq. 5}$$

This step is important to improve the accuracy in demarcating the *ab* complex in APG signals. It is clear from Figures 7 (d) and 9 (d) that applying the square to APG signals measured at rest and after exercise magnifies *a* waves compared to the other APG features.

### Generating Blocks of Interest

Since the *a* wave shape and duration is similar to the QRS complex in ECG signals, the onset and offset of the potential *a* waves will be demarcated using two moving averages [22-25]:

- i) First moving average ( $MA_{Peak}$ ):** is used to emphasise the *a* wave area, shown as the dotted line in Figure 7 (e) for APG signal measured before exercise, and in Figure 9 (e) for the APG signals measured after exercise.

$$MA_{Peak}[n] = \frac{1}{W_1} (y[n - (W_1 - 1)/2] + \dots + y[n] + \dots + y[n + (W_1 - 1)/2]) \quad \text{Eq. 6}$$

where  $W_1 = 111 \text{ms} * SF$ , which is the window width of the average  $a$  wave duration. Its value is rounded to the nearest odd integer.

**ii) Second Moving Average ( $MA_{OneBeat}$ ):** is a threshold for the first moving average, shown as the solid line in Figure 7 (e) and 9 (e) for APG signal measured before and after exercise.

$$MA_{OneBeat}[n] = \frac{1}{W_2} (y[n - (W_2 - 1)/2] + \dots + y[n] + \dots + y[n + (W_2 - 1)/2]) \quad \text{Eq. 7}$$

where  $W_2 = 694 \text{ms} * SF$  is the window width of approximately one beat duration. Its value is rounded to the nearest odd integer.

### **The moving averages alignment**

At rest, the signals generated from the two filters are not aligned as shown in Figure 6 (e); however, the signals are aligned as shown in Figure 9 (e). This means that the window size ( $W_2$ ) of the second moving average ( $MA_{OneBeat}$ ) is slightly large for the APG signal measured at rest. The heart beat interval decreases with exercise when the heart rate increases. The window size  $W_2$  is adjusted to 597 ms (as done for QRS complex detection) to demarcate heartbeats in the APG signals before and after exercise. The different alignment between  $MA_{Peak}$  and  $MA_{OneBeat}$ , as shown in Figure 7 (e), did not affect the beat demarcation process. Conversely, it demarcated the  $a$  waves successfully, as shown in Figure 7 (f).

### *Thresholding*

An offset will be used to improve the detection accuracy [22-25]. The equation that determines the offset level ( $\alpha$ ) is  $\alpha = \beta \bar{z}$ , where  $\beta$  is 10 per cent, as used for ECG signal algorithms, while  $\bar{z}$  is the statistical mean of the squared filtered APG signal ( $z$ ).

The first dynamic threshold value  $THRI$  is calculated by shifting the  $MA_{OneBeat}$  signal with an offset level  $\alpha$ , as follows:

$$THRI = MA_{OneBeat}[n] + \alpha \quad \text{Eq. 8}$$

In this stage, the blocks of interest will be generated by comparing the  $MA_{Peak}$  signal with  $THRI$ . If a block is higher than  $THRI$ , it is classified as a block of interest containing an APG feature ( $a$  wave or  $e$  wave) or perhaps noise. As the algorithm ignores the signal below the zero level, the blocks will almost never contain  $b$ ,  $c$ , or  $d$  waves, as shown in Figure 10 (b).

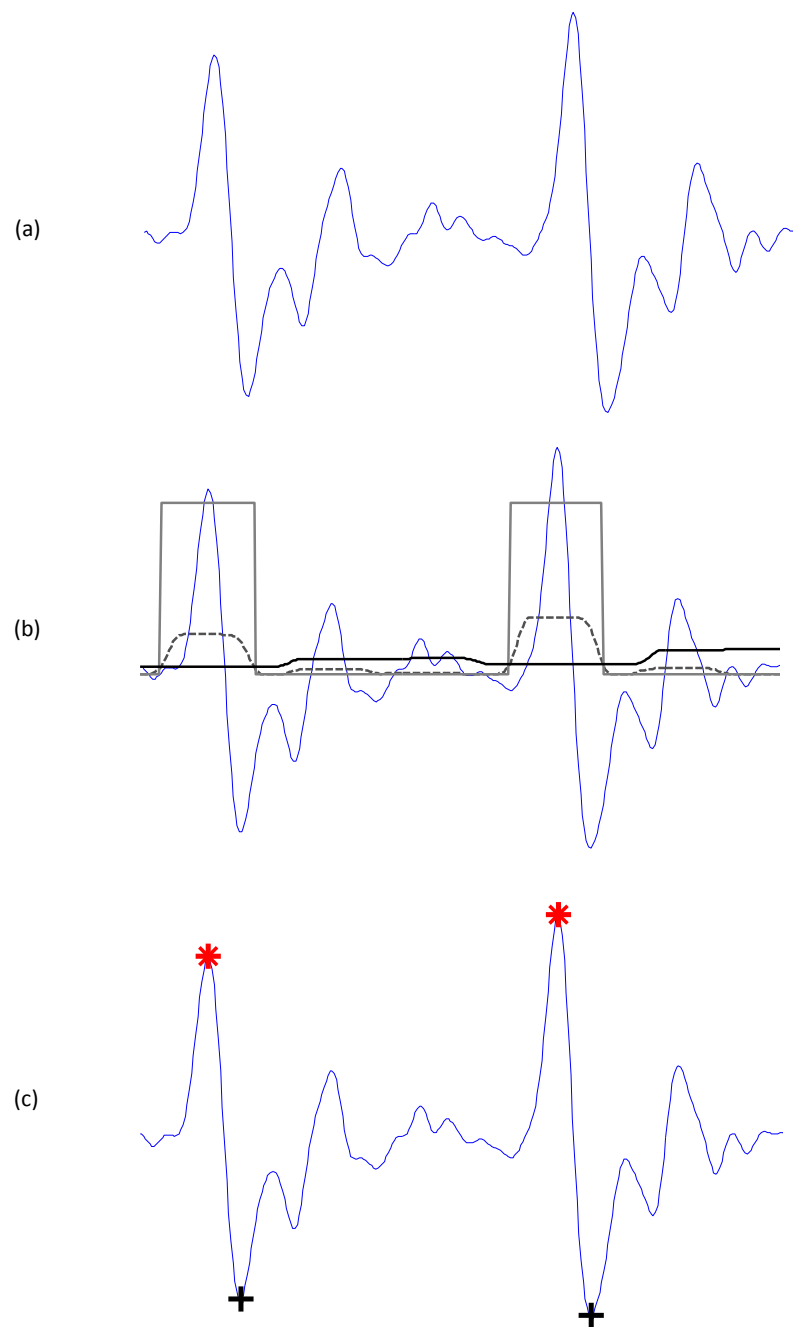


**Figure 10** Demonstrating the effectiveness of using two moving averages to detect *a* and *b* waves. (a) Filtered APG signal with Butterworth bandpass filter (b) generating blocks of interest after using two moving averages: the solid line is the first moving average and the dotted line is the second moving average (c) the detected *a* and *b* waves after applying the thresholds.

```

IF  $MA_{peak}[n] > THR1$  THEN
     $Blocks[n] = 1$ 
ELSE
     $Blocks[n] = 0$ 
END

```

By this stage, many blocks of interest have been generated. Therefore, the next step is to reject the blocks that result from noise. The rejection should be related to the anticipated block width.

In this paper, the undesired blocks are rejected using a threshold called  $THR2$ , which rejects the blocks that contain  $d$  wave and noise. By applying the  $THR2$  threshold, the accepted blocks will contain  $a$  waves only.

$$THR2 = W_i \quad \text{Eq. 9}$$

As discussed, threshold  $THR2$  corresponds to the anticipated  $a$ -wave duration. If a block is higher than  $THR2$ , it is classified as an  $a$  wave. If not, it will be classified as noise. The last stage is to find the maximum absolute value within each block to detect the  $a$ -peaks.

Two consecutive  $aa$  intervals are shown in Figure 10 (b) to demonstrate the idea of using two filters to generate blocks of interest. Not all of the blocks are potential  $a$  waves; some blocks are caused by noise and need to be eliminated.

The blocks associated with small width are considered blocks caused by noise. Blocks that are less than half of the expected size for the  $a$  wave duration are rejected. The expected size for the  $a$  wave duration is based on the statistics for healthy adults, as described above. Blocks that are smaller than the expected width for the  $a$  wave duration will be rejected. The rejected blocks are considered as noisy blocks and the accepted blocks are considered to contain an  $a$  wave.

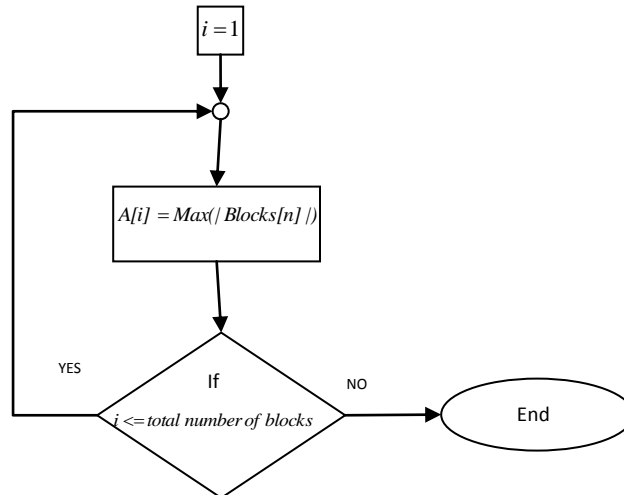


**Figure 11 Flowchart for detecting  $a$  waves.** This loop searches for the maximum absolute amplitude within each accepted block to be considered as an  $a$  wave.

## 7) Detect *a* Wave

The maximum absolute value within each accepted block is considered the *a* peak. As shown in Figure 11, the *a* wave detection loop starts with the first block, when  $i = 1$  until it finishes all accepted blocks provided from the previous step. Each time a block is processed, the maximum amplitude value within is considered an *a* wave. The result of this loop will be that all detected *a* waves will be stored in array *A*.

## 8) Detect *b* Wave

As shown in Figure 12 (a), the *b* wave in a healthy person is the global minimum. In an unhealthy person (see Figure 12 (b)), the *d* wave is the global minimum. However, in both cases, the *b* wave is the first local minimum after the *a* wave. The *b* wave can therefore be detected by finding the local minimum, as follows:

$$|APG(i)| > |APG(i+1)| \text{ and } |APG(i)| > |APG(i-1)|$$

where APG is the current *aa* interval (see Figure 12) and '*i*' is the samples counter.

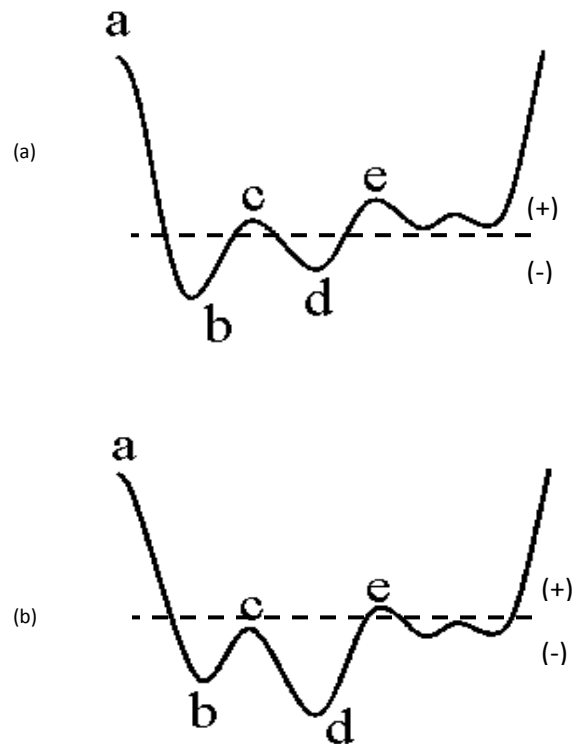


**Figure 12** Demonstrating the local minimum and global minimum of the *b* wave in the APG signal [26]. (a) In a healthy person, the *b* wave is the global minimum, (b) in an unhealthy person, the *b* wave is the local minimum.

As discussed above, the normal limit of the  $b$  wave width for a healthy adult is  $97 \pm 13$  ms. Therefore, the samples counter ' $i$ ' starts with 8 ms after the  $a$  peak and ends with 81 ms, as shown in Figure 13. Once the local minima has been found the loop ends.

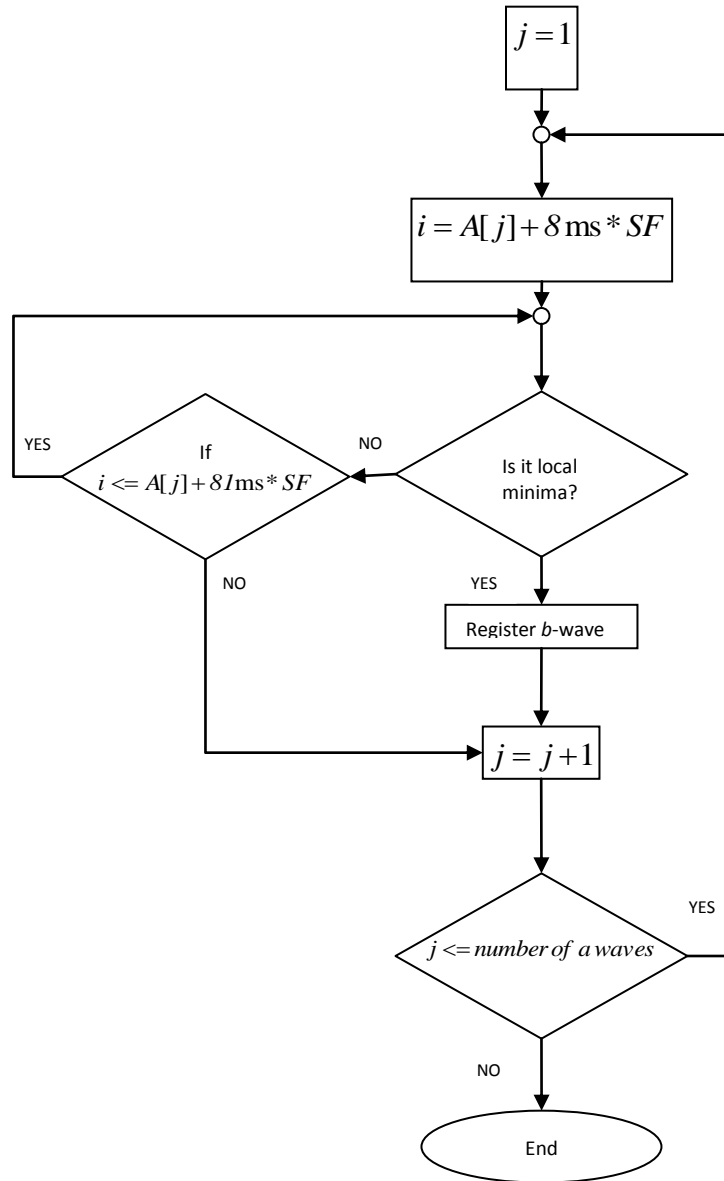


**Figure 13 Flowchart for  $b$  waves detection.** This loop searches for  $b$  waves regarding the  $a$  wave location. The first minimum value is considered the  $b$  wave, for both healthy and unhealthy candidates. The variable ' $j$ ' is a counter for  $a$  waves, while the variable ' $i$ ' is a counter to search for  $b$  waves, where  $SF$  is the sampling frequency of the processed signal.

**Table 1 A Rigorous optimisation over all parameters of the *a* detection algorithm: frequency band, *W1*, *W2*, and the offset.** All possible combinations of parameters (5,610 iterations) have been investigated and sorted in descending order according to their overall accuracy. The database used is PPG-Firefighters Heat Stress database. The overall accuracy is the average value of SE and +P.

Iterations	Frequency Band	W1	W2	Offset (per cent)	SE (per cent)	+P (per cent)	Overall Accuracy (per cent)
1	0.5-7 Hz	40	250	10	98.72	99.46	99.09
2	0.5-7 Hz	40	250	8	98.61	99.57	99.09
3	0.5-7 Hz	40	250	9	98.61	99.57	99.09
4	0.5-7 Hz	40	250	7	98.53	99.57	99.05
5	0.5-8 Hz	40	250	9	98.62	99.46	99.04
6	1-8 Hz	40	250	10	98.62	99.36	98.99
7	0.5-8 Hz	40	250	9	98.27	99.70	98.99
8	0.5-8 Hz	40	250	7	98.39	99.57	98.98
9	0.5-8 Hz	40	250	8	98.39	99.57	98.98
10	1-8 Hz	40	250	8	98.18	99.70	98.94
11	0.5-7 Hz	35	250	9	98.16	99.70	98.93
12	0.5-7 Hz	35	250	10	98.16	99.70	98.93
13	1-9 Hz	40	250	10	98.37	99.49	98.93
14	0.5-8 Hz	40	250	6	98.16	99.70	98.93
15	1-8 Hz	40	250	10	98.35	99.49	98.92
16	0.5-8 Hz	35	250	10	98.14	99.70	98.92
17	0.5-9 Hz	35	250	8	98.14	99.70	98.92
18	0.5-7 Hz	40	250	6	98.18	99.57	98.88
19	0.5-8 Hz	40	250	5	98.05	99.70	98.87
20	0.5-9 Hz	35	250	9	98.14	99.59	98.87
•	•	•	•	•	•	•	•
•	•	•	•	•	•	•	•
•	•	•	•	•	•	•	•
5606	0.5-7 Hz	20	200	1	55.38	99.41	77.39
5607	0.5-9 Hz	20	200	0	55.35	99.31	77.33
5608	1-8 Hz	20	200	0	54.75	99.51	77.13
5609	0.5-8 Hz	20	200	0	54.46	99.31	76.89
5610	0.5-7 Hz	20	200	0	53.84	99.31	76.58

The detected *a* and *b* waves are compared to the annotated *a* and *b* waves to determine whether they were detected correctly.

The following statistical parameters were used to evaluate the algorithm:

$$Se_{a/b} = \frac{TP_{a/b}}{TP_{a/b} + FN_{a/b}} \quad \text{Eq. 10}$$

$$+P_{a/b} = \frac{TP_{a/b}}{TP_{a/b} + FP_{a/b}} \quad \text{Eq. 11}$$

True positive ( $TP_{a/b}$ ): *a/b* wave classified as *a/b* wave.

False positive ( $FP_{a/b}$ ): non- *a/b* wave classified as *a/b* wave.

False negative ( $FN_{a/b}$ ): *a/b* wave misclassified.

The sensitivity  $Se_{a/b}$  is the percentage of true  $a/b$  waves that were correctly detected by the algorithm. The positive predictivity  $+P_{a/b}$  is the percentage of detected  $a/b$  waves that are real  $a/b$  waves.

Remarks on the  $a$  wave detection algorithm:

Any change in the  $a$  wave algorithms's parameters (frequency band, event duration and offset  $\alpha$ ) will affect the overall performance of the proposed algorithm. A rigorous investigation of all interrelated parameters is shown in Table 1. Optimisations of the beat detector's spectral window for lower frequency were within 0.5–1 Hz with higher frequency within 7–15 Hz. All combinations of the frequency band 0.5–15 Hz have been explored. The window size of the first moving average ( $W_1$ ) changed from 55 ms to 111ms, whereas the window size of the second moving average ( $W_2$ ) changed from 555 ms to 694 ms. The offset tested over the range 0–10 per cent of the mean value of the squared filtered ECG signal.

It is clear from Table 1 that the optimal frequency range for the  $a$  detection algorithm over the PPG-Firefighters database is 0.5–7 Hz, as proposed by Benitez et al. [27]. Moreover, the optimal values for the moving averages and offset are  $W_1 = 111ms * SF \equiv 40$ ,  $W_2 = 694ms * SF \equiv 250$  and  $\alpha = 0.1 * \bar{z}$ .

The proposed algorithm was tested on the PPG–Army Heat Stress Dataset. As mentioned above, this dataset contains 27 APG recordings measured before and after exercise. The main objective behind testing the algorithm against the APG measured after exercise is to test the robustness of the algorithm against non-stationary effects, low SNR, and high heart rate. All the reasons for detection failure are described in detail, as follows.

**1) Stationarity.** analysing a stationary APG signals is straightforward. As  $a$  waves have similar amplitudes, the signal's statistical characteristics (i.e. mean and standard deviation) do not change with time, and a simple level threshold can effectively detect  $a$  and  $b$  waves. Figures 14 (a) and 15 (a) represent the APG signals with stationarity effects for volunteer I2 (before exercise) and G2 (after exercise) (all  $a$  waves are almost straight-lined).

It is anticipated that a simple detection algorithm can detect  $a$  and  $b$  waves in stationary APG signals at rest and after exercise. The proposed algorithm detected the  $a$  and  $b$  waves correctly in stationary APG signals, as expected.

**2) Non-stationarity.** processing non-stationary APG signals is difficult, as the statistical characteristics' standard deviation changes with time ( $a$  waves amplitude vary with time and simple level thresholds cannot optimally detect  $a$  and  $b$  waves). This will undoubtedly have a negative effect on the performance of the detection algorithm used. However, the proposed algorithm detected the  $a$  and  $b$  waves correctly in non-stationary APG signals before exercise (as shown in Figures 14 (c,d)), and after exercises (as shown Figures 15 (c,d)). It is clear that non-stationarity in APG signal processing is challenging, especially with APG signals after exercises.

**3) Low amplitude.** the APG signals for volunteers O2 (before exercise) and for volunteer B2 (after exercise) have low amplitude. The normal level for APG signals is usually in volts (as shown in Figures 14 (a,c) and 14 (a-d)). However, the amplitudes are occasionally in millivolts (as shown in Figures 14 (b,d)). Certainly, applying a simple level threshold is not a valid solution. The proposed algorithm handled very poor amplitudes very well (as shown in Figure 14 (b)). It is clear that the proposed algorithm is amplitude-independent and is able to detect the  $a$  and  $b$  waves in millivolts and microvolts.

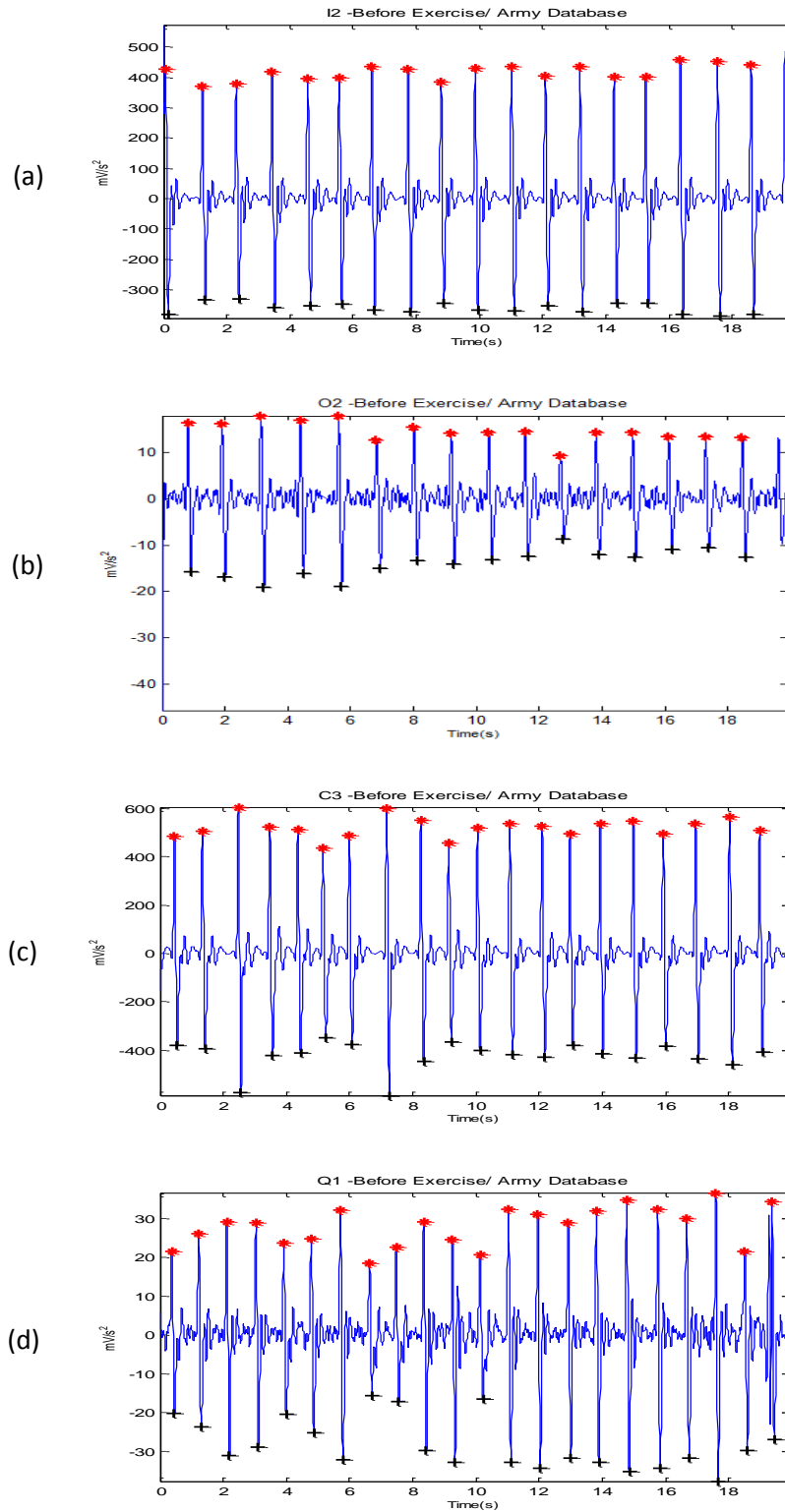


**Figure 14 Detected  $a$  and  $b$  waves in APG signals before exercise.** It contains (a) Stationary signals, (b) low amplitudes, (c) irregular heart rhythm, (d) high-frequency noise. ‘\*’ represents the  $a$  wave and ‘+’ represents the  $b$  wave.

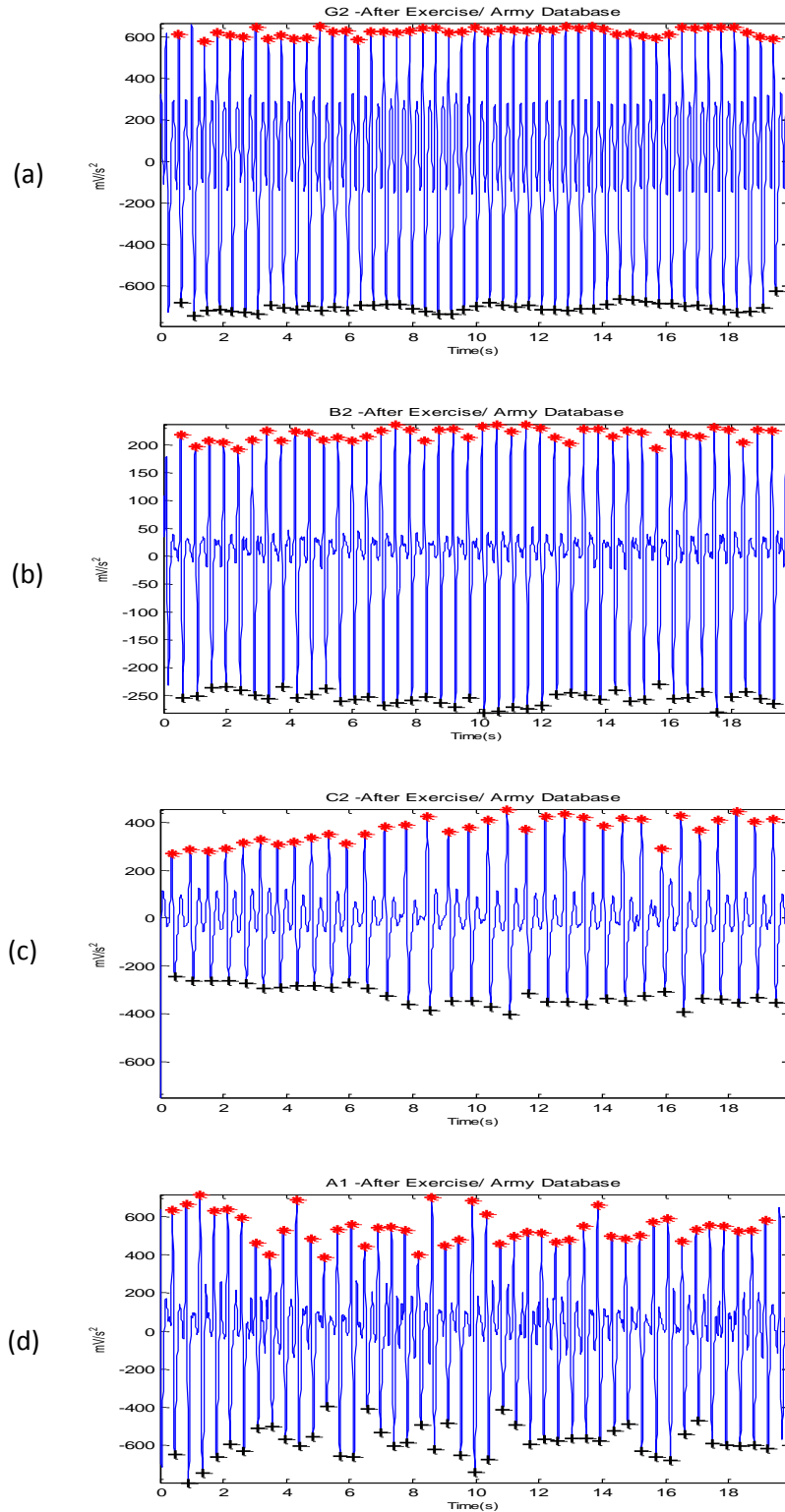


**Figure 15. Detected  $a$  and  $b$  waves in APG signals after exercise.** It contains (a) Stationary signals, (b) low amplitudes, (c) irregular heart rhythm, (d) high-frequency noise. ‘\*’ represents the  $a$  wave and ‘+’ represents the  $b$  wave.

**4) Regular heart rhythm.** this is called NSR in ECG signals [28]. A normal heartbeat is called regular when the rhythm is constant and the occurrence of the next beat is predictable. The analysis of a regular heart rhythm is simple, as the *a* waves are repeated with an equally spaced pattern. This regularity helps the time-domain threshold methodologies to detect *a* and *b* waves successfully.

The proposed algorithm detected the *a* and *b* waves correctly in APG signals with a regular heart rhythm as shown in Figures 14 (a,d) and 15 (a,d), even in records with low amplitudes, as shown in Figures 14 (b) and 15 (b).

**5) Irregular heart rhythm.** the sensation of an irregular heart rhythm is usually related to either premature beats or atrial fibrillation. The proposed algorithm successfully detected the *a* and *b* waves with premature beats in both conditions—at rest and after exercise (see Figures 14 (c) and 15 (c)).

**6) High frequency noise.** Figures 14 (d) and 15 (d) illustrate the robustness of the proposed algorithm against noise.

Although the duration of the *a* and *b* waves changed dramatically after exercise, the proposed algorithm succeeded in detecting the *a* and *b* waves efficiently.

As discussed above, the proposed method successfully detected *a* and *b* waves in APG signals with a low SNR, non-stationarity, irregular heart rhythms, and before and after exercise (see Figures 14 and 15).

**Table 2 *a, b* wave detection performance on PPG–Army Heat Stress Database**

Record	Before Exercise						After Exercise					
	No of beats	TP <sub>a/b</sub>	FP <sub>a/b</sub>	FN <sub>a/b</sub>	Se (%)	+P (%)	No of beats	TP <sub>a/b</sub>	FP <sub>a/b</sub>	FN <sub>a/b</sub>	Se (%)	+P (%)
A1	26	26	0	0	100.00	100.00	45	44	1	0	100.00	97.78
A2	24	24	0	0	100.00	100.00	44	44	0	0	100.00	100.00
B1	17	17	0	0	100.00	100.00	36	36	0	0	100.00	100.00
B2	26	26	0	0	100.00	100.00	43	43	0	0	100.00	100.00
C2	20	20	0	0	100.00	100.00	33	33	0	0	100.00	100.00
C3	20	20	0	0	100.00	100.00	30	30	0	0	100.00	100.00
D2	22	22	0	0	100.00	100.00	33	33	0	0	100.00	100.00
D3	19	19	0	0	100.00	100.00	23	23	0	0	100.00	100.00
E1	22	22	0	0	100.00	100.00	25	25	0	0	100.00	100.00
E2	22	22	0	0	100.00	100.00	25	25	0	0	100.00	100.00
E3	19	19	0	0	100.00	100.00	34	34	0	0	100.00	100.00
G2	30	30	0	0	100.00	100.00	48	40	8	0	100.00	83.33
G3	19	19	0	0	100.00	100.00	33	33	0	0	100.00	100.00
H3	23	23	0	0	100.00	100.00	31	31	0	0	100.00	100.00
I1	22	22	0	0	100.00	100.00	30	30	0	0	100.00	100.00
I2	17	17	0	0	100.00	100.00	28	28	0	0	100.00	100.00
J2	23	23	0	0	100.00	100.00	36	36	0	0	100.00	100.00
L2	24	24	0	0	100.00	100.00	36	36	0	0	100.00	100.00
L3	24	24	0	0	100.00	100.00	35	35	0	0	100.00	100.00
N2	18	18	0	0	100.00	100.00	23	23	0	0	100.00	100.00
N3	20	20	0	0	100.00	100.00	29	29	0	0	100.00	100.00
O1	24	24	0	5	82.76	100.00	29	29	0	0	100.00	100.00
O2	17	17	0	0	100.00	100.00	32	32	0	0	100.00	100.00
P1	26	26	0	0	100.00	100.00	35	35	0	0	100.00	100.00
P2	20	20	0	0	100.00	100.00	29	29	0	0	100.00	100.00
Q1	22	21	1	0	100.00	95.45	27	27	0	0	100.00	100.00
Q2	18	18	0	0	100.00	100.00	33	33	0	0	100.00	100.00
<sup>27</sup> volunteers	584	583	1	5	99.36	99.83	885	876	9	0	100.00	99.30

Table 2 represents the  $a$  and  $b$  wave detection rates respectively. As the detection of  $b$  waves depends on the detection of  $a$  waves, one table will therefore contain both results.

As shown in Table 2, few FNs occur. Record Q1 (before exercise) has relatively high-frequency noise, resulting in one FN. The number of FPs were 8 because of high amplitude of  $e$  waves. The overall average sensitivity for  $a$  and  $b$  wave detection (before and after exercise) was 99.68 per cent and positive predictivity was 99.57 per cent.

Due to the dominant  $a$  peaks and merged  $c,d$ , and  $e$  waves in APG signals measured after exercise, the algorithm performed more efficiently with recordings measured after exercise compared to records measured at rest.

### Comparison of a Detection Performance on PPG-Army Dataset

The performance of the proposed algorithm is compared to the nine algorithms used by Matsuyama [19] and applied to the same database. As shown in Table 3, the proposed algorithm scored the highest sensitivity and positive predictivity rates among the nine algorithms.

**Table 3  $a$  wave detection rates using the nine algorithms with optimal thresholds [19]**

Algorithm	$TP_a$ (%)	$FN_a$ (%)	$FP_a$ (%)	$Se_a$ (%)	$+P_a$ (%)	Threshold Values		
						Th1	Th2	Th3
<b>Proposed algorithm</b>	99	0.7	0.4	99.68	99.57	Dynamic event related threshold		
<b>AF1</b>	69.5	7.5	30.5	90.25	69.5	0.31	0.0001	-0.001
<b>AF2</b>	0.018	0.27	99.98	6.25	0.018	0.21	0.75	-
<b>AF3</b>	0	0	100	NA	0	62	-	-
<b>FD1</b>	0.27	2.8	99.73	8.79	0.27	0.099	-	-
<b>FD2</b>	0	0	100	NA	0	150	-	-
<b>DF1</b>	0	0	100	NA	0	21	-	-
<b>DF2</b>	48.8	14.2	51.2	77.46	48.8	1	0.06	-
<b>FS1</b>	2.42	0.3	97.58	88.97	2.42	154.5	-	-
<b>FS2</b>	42.46	6.9	57.54	86.02	42.46	0.55	0.47	-

### Conclusion

The detection algorithms of  $a$  and  $b$  waves in APG signals can hardly be found in literature. However, a promising algorithm has been proposed to detect  $a$  and  $b$  waves simultaneously and robustly against high-frequency noise, low amplitude, non-stationary effects and irregular heartbeats in APG signals measured before and after exercise. This numerically-efficient algorithm was evaluated using 27 records, containing 1,469 heartbeats resulting in 99.68 percent sensitivity and 99.57 percent positive predictivity.

The accurate detection of  $a$  and  $b$  waves in the APG offers a non-invasive method of evaluating cardiac functioning. The usage of APG can be useful for heart-rate-variability analysis and identification of individuals at risk and may replace the existing some of the current traditional cardiovascular diagnostic tools.

### Acknowledgement

Mohamed Elgendi would like to gratefully acknowledge the Australian government and Charles Darwin University whose generous scholarships facilitated this research. He would like also to thank Prof. Friso De Boer and Mrs. Mirjam Jonkman for their valuable comments and annotation of the used dataset. He also would like to thank Dr Gari Clifford for helpful discussions.

## References

1. Kimm SY, P.G., Stylianou MP, Waclawiw MA, Lichtenstein C *National trends in the management of cardiovascular disease risk factors in children: second NHLBI survey of primary care physicians.* Pediatrics, 1998; 102:E50.
2. Strong JP, M.G., McMahan CA, Tracy RE, Newman WP, Herderick EE, Cornhill JF . *Prevalence and extent of atherosclerosis in adolescents and young adults. Implications for prevention from the pathobiological determinants of atherosclerosis in young study.* JAMA 1999; 281:727-737.
3. Leeson CP, W.P., Cook DG, Mullen MJ, Donald AE, Seymour CA, Deanfield JE *Cholesterol and arterial distensibility in the first decade of life: a population-based stud.* Circulation 2000; 101:1533-1538.
4. Chrife R, P.V., Spodick DH *Measurement of the left ventricular ejection by digital plethysmography.* American Heart Journal, 1971(82:222-227).
5. Kelly RP, H.C., Avolio AP, O'Rourke MF, *Noninvasive determination of age-related changes in the human arterial pulse.* Circulation, 1989; 80:1652-1659.
6. O'Rourke MF, K.R., Avolio AP, *The arterial pulse.* Philadelphia : Lea & Febiger, 1992: 3-14.
7. Darne BM, G.X., Safar ME, Cambien FA, Guize L *Pulsatile versus steady component of blood pressure. A cross-sectional and prospective analysis on cardiovascular mortality.* Hypertension, 1989; 13:392-400.
8. Kelly RP, H.C., Kerber S, Vielhauer C, Hoeks AP, Zidek W, Rahn KH, *Different effects of hypertension, atherosclerosis and hyperlipidemia on arterial distensibility.* Hypertension, 1995; 13:1712-1717.
9. Takazawa K, T.N., Fujita M, Matsuoka O, Saiki T, Aikawa M, Tamura S, Ibukiyama C, *Assessment of vascular agents and vascular aging by the second derivative of photoplethysmogram waveform.* Hypertension, 1998; 32:365-370.
10. Bortolotto LA, B.J., Kondo T, Takazawa K, Safar ME *Assessment of vascular aging and atherosclerosis in hyperetensive subjects: second derivative of photoplethysmogram versus pulse wave velocity. .* Hypertension 2000; 13:165-171.
11. Elgendi, M., *Standard Terminologies for Photoplethysmogram Signals.* Current Cardiology Reviews, 2012; 8(3): 215-219.
12. Fitchett, D.H., *Forearm arterial compliance: a new measure of arterial compliance? .* Cardiovascular Research, 1984; 18:651-656.
13. Seki, H., *Classification of wave contour by first and second derivative of plethysmogram (in Japanese).* Pulse Wave, 1977; 7:42-50.
14. Ozawa, T., *Pattern of second derivative of volume pulse wave, the relation between non-invasive index of ventricular function and peak acceleration and effect of preloading to peak velocity (in Japanese).* Pulse Wave 1978; 8:22-31.
15. Takazawa K, F.M., Kiyoshi Y, Sakai T, Kobayashi T, Maeda K, Yamashita Y, Hase M, Ibukiyama C, *Clinical usefulness of the second derivative of a plethysmogram (acceleration plethysmogram).* Cardiology, 1993; 23:207-217.
16. Takada H, W.K., Harrel JS, Iwata H *Acceleration plethysmography to evaluate aging effect in cardiovascular system. Using new criteria of four wave patterns. .* Medical Progress through Technology, 1996; 21:205-210.
17. Imanaga I, H.H., Koyanagi S, Tanaka K *Correlation between wave components of the second derivative of plethysmogram and arterial distensibility.* Jpn Heart J 1998; 39:775-784.

18. Elgendi, M., *On the Analysis of Fingertip Photoplethysmogram Signals*. Current Cardiology Reviews, 2012; **8**(1): 14-25.
19. Matsuyama, A., *ECG and APG Signal Analysis during Exercise in a Hot Environment*, in *School of Engineering and Information Technology*, 2009; Charles Darwin University: Darwin, Australia.
20. Friesen, G.M., Jannett, T.C., Jadallah, M.A., Yates, S.L., Quint, S.R., and Nagle, H.T., *A comparison of the noise sensitivity of nine QRS detection algorithms*. Biomedical Engineering, IEEE Transactions on, 1990; **37**(1): 85-98.
21. Oppenheim, A. and Shafer, R., (eds). *Discrete-time Signal Processing* NJ: Prentice Hall; 1989.
22. Elgendi, M., Jonkman, M., and De Boer, F. *Applying the APG to measure Heart Rate Variability*. Proceedings of The 2nd International Conference on Computer and Automation Engineering, 2010; Singapore.
23. Elgendi, M., Jonkman, M., and De Boer, F., *Heart Rate Variability and Acceleration Plethysmogram measured at rest*, in *Biomedical Engineering Systems and Technologies*, A. Fred, J. Filipe, and h. Gamboa, Editors. 2011, Springer. p. 266-277.
24. Elgendi, M., Jonkman, M., and De Boer, F. *Heart Rate Variability Measurement Using the Second Derivative Photoplethysmogram*. Proceedings of The 3rd International Conference on Bio-inspired Systems and Signal Processing (BIOSIGNALS2010), 2010; Spain.
25. Elgendi, M., Jonkman, M., and De Boer, F. *Measurement of a-a Intervals at Rest in the Second Derivative Plethysmogram*. Proceedings of IEEE Conference in Bioelectronics and Bioinformatics, 2009; RMIT University, Melbourne.
26. Tokutaka, H., Maniwa, Y., Gonda, E., Yamamoto, M., Kakihara, T., Kurata, M., Fujimura, K., Shigang, L., and Ohkita, M., *Construction of a General Physical Condition Judgment System Using Acceleration Plethysmogram Pulse-Wave Analysis*. Springer Berlin / Heidelberg, 2009; **5629**: 307-315.
27. Arzeno, N., Deng, Z., and Poon, C., *Analysis of First-Derivative Based QRS Detection Algorithms*. IEEE Transactions on Biomedical Engineering, 2008; **55**(2): 478-484.
28. Braunwald, E., Zipes, D., Libby, P., and Bonow, R., (eds). *Braunwald's Heart Disease: A Textbook of Cardiovascular Medicine* (7th edition), Philadelphia: Saunders; 2004.